Periodicals of Engineering and Natural Sciences ISSN 2303-4521
Vol.5, No.2, June 2017, pp. 237~244
Available online at: http://pen.ius.edu.ba

Raman and FT-IR Spectra, DFT and SQMFF calculations for N,N-Dimethylaniline

Berna Çatıkkaş
Department of Physics, Mustafa Kemal University

Article Info

Article history:

Received May 30th, 2017
Revised June 15th, 2017
Accepted June 17th, 2017

Keyword:

Monoazo disperse dye
Infrared and Raman Spectroscopy
Scaled Quantum Mechanical Force Field (SQMFF)

ABSTRACT

Raman and FT-IR spectra of N,N-Dimethylaniline (DMA) molecule, which is a monoazo disperse dye, were recorded in the regions of 0 to 2085 cm^{-1} (Raman) and 350-4000 cm^{-1} (FT-IR). Vibrational frequencies calculation and molecular electronic potential surface have been computed by using density functional B3LYP method with the 6-31+G(d,p) set for the ground state geometry of the title molecule. Total potential energy distributions (TED) was obtained with Scaled Quantum Mechanical calculations to make the fundamental assignment. Assigned fundamental modes of DMA molecule were compared with the previous reported experimental values.

Corresponding Author:

Berna Çatıkkaş,
Department of Physics,
Mustafa Kemal University,
Tayfur Sökmen Campus, Antakya 31034, Hatay, TURKEY.
Email: berna@mku.edu.tr

1. Introduction

For dying of natural and synthetic fibres are widely used azo dyes [1], [2]. For example, disperse dyes using has been continuously increasing in the textile industry after the discovery of synthetic fibres [1]. Also, many high technology fields are using azo dyes, such as electronic devices, linear and nonlinear optics, reprography, sensors. Disperse dyes are the most important dyes group for dyeing of hydrophobic fibers [3]–[5]. Molecular structure analysis of a monoazo disperse dye, N,N-dimethylaniline (DMA, as shown Fig. 1) molecule was fully characterized by Arslan et al. [6].

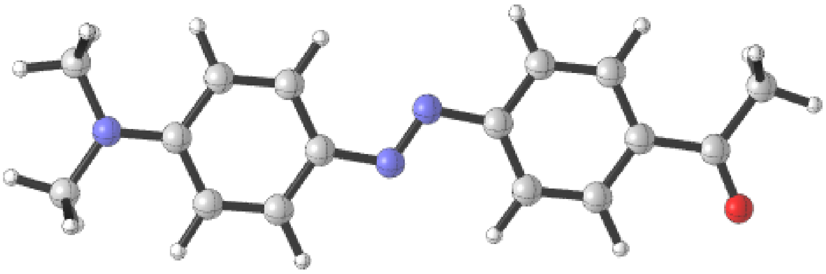

Figure 1. The optimized molecular structure of the DMA molecule (The structure were drawn using CYLview 1.0b [7]).

Calculated and experimental IR and Raman spectrums show that the all-inclusive picture on electronic possessions [8] and the correct structure information about the studied molecule. Vibrational frequencies investigation and detail IR and Raman spectroscopy analysis help for proper assignments of compound molecules. Then, the complete vibrational assignments and the simulated IR-Raman spectra of the fundamentals were constructed by using Density Functional Theory (DFT) and the scaled quantum mechanical force fields (SQMFF) procedure product of its potential energy distribution values.

2. Material and method

2.1. Experimental

The Infrared (IR) spectrum was recorded in the region 350-4000 cm^{-1} by using Perkin Elmer Spectrum Two with U-ATR FTIR spectrometer. In this study, the Raman spectrum was measured by using Renishaw inVia confocal Raman microscope (Gloucestershire, UK) and a near infrared diode laser (785 nm) maximum at 500mW, 1200 lines/mm source. A 1024×256 pixels CCD array detector detected Raman scattering signals. Raman range from 0 to 2085 cm^{-1} was detected with a 50× objective.

2.2. Computation

In this work, the calculations were carried out optimized geometry, fundamental frequencies and a map of molecular electrostatic potential calculations by using DFT the B3LYP method and 6-31+G(d,p) basis set by utilizing the Gaussian 09 W [9] program package for studied molecule. The frequency calculations showed that the structure is in the state of the true minimum of potential energy.
The cartesian coordinates force fields were converted to the internal coordinates [10], [11] for the corresponding optimized structure. In the scaled quantum mechanical force fields [12] methodology, an internal coordinate representation of the cartesian force constants, which are obtained using B3LYP/6-31+G(d,p) level. Then the elements of the internal force constant matrix (F_{ij}(scaled)) are scaled based on scaled factors (s_i and s_j),

$$F_{ij}(\text{scaled})=(s_i)^{1/2}F_{ij}(s_j)^{1/2} \quad (1)$$

In this study, initial scaling factors (s_i) are used as recommended by Baker [13], [14] in Table 1. Then direct scaling of the $F=[F_{ij}]$ matrix is used for fitting the calculate fundamental wavenumbers to the corresponding experimental.

$$F_{ij}=(s_i\, s_j)^{1/2}F_{ij} \quad (2)$$

Table 1. Using initial scale factors (s_i)

Vibrations		Bonds	Scale factor
Stretching	1	C-N, N-N, C-O	0.9207
	2	C-H	0.9264
Bending	3	C-C-H	0.9431
	4	C-X-X	1.0144
Torsion	5	X-X-X-X	0.9523

Scaling factor optimization method is defined by merit function [14];

$$\chi^2(s_i) = \sum\{[v_i^{exp} - v_i^{theor}(s_i)]w_i\}^2 \quad (3)$$

In addition, the total energy distribution (TED) is determined stretching, bending or torsion percentages contribute to a particular normal mode. The Infrared and Raman spectrum were plotted in terms of Gaussian band shapes with 7 cm^{-1} bandwidth by using the SQM outputs. For scaling to getting these internal coordinate force were carried out with the scaled quantum mechanical force fields procedure by utilizing the Parallel Quantum Solutions (PQS) program [15].
Molecular electrostatic potential V(r) is defined by the electronic density function: $\rho(r')$ and Z_A is the charge on the nucleus A, located at R_A[16]–[18].

$$V(r) = \sum_A \frac{Z_A}{(R_A-r)} - \int \frac{\rho(r')}{(r'-r)} d(r') \quad (4)$$

To observe and get information about variably charged regions of the molecule, the map of molecular electrostatic potential was investigated using theoretical calculations.

3. Results and discussion

3.1. Vibrational assignments

The computed vibrational assignments were used for identifying the vibrational modes clearly in Fig.2., Fig.3. and Table 2. In this study, all weighted 105 fundamental frequencies RMS and mean average deviation are 7.46 and 3.78 respectively. The RMS values of the calculated SQM in the pre-fingerprint region (<500 cm^{-1}), fingerprint region (500-2500 cm^{-1}) and post-fingerprint region (>2500 cm^{-1}) are 3.45, 6.89 and 15.57, respectively. Hence, overall agreement between the SQM and experimental frequencies can be made with confidence. The both experimental and calculated IR and Raman spectrum of the title compounds are graphically illustrated in Fig. 2. and Fig. 3. The calculated SQMFF Raman and IR absorption spectrum bandwidth were plotted with 4 cm^{-1} in this study (in Fig. 2 and 3). The observed and calculated vibrational frequencies with the TED assignments were given in Table 2. Discussion for the characteristic spectral region is summarized as below.

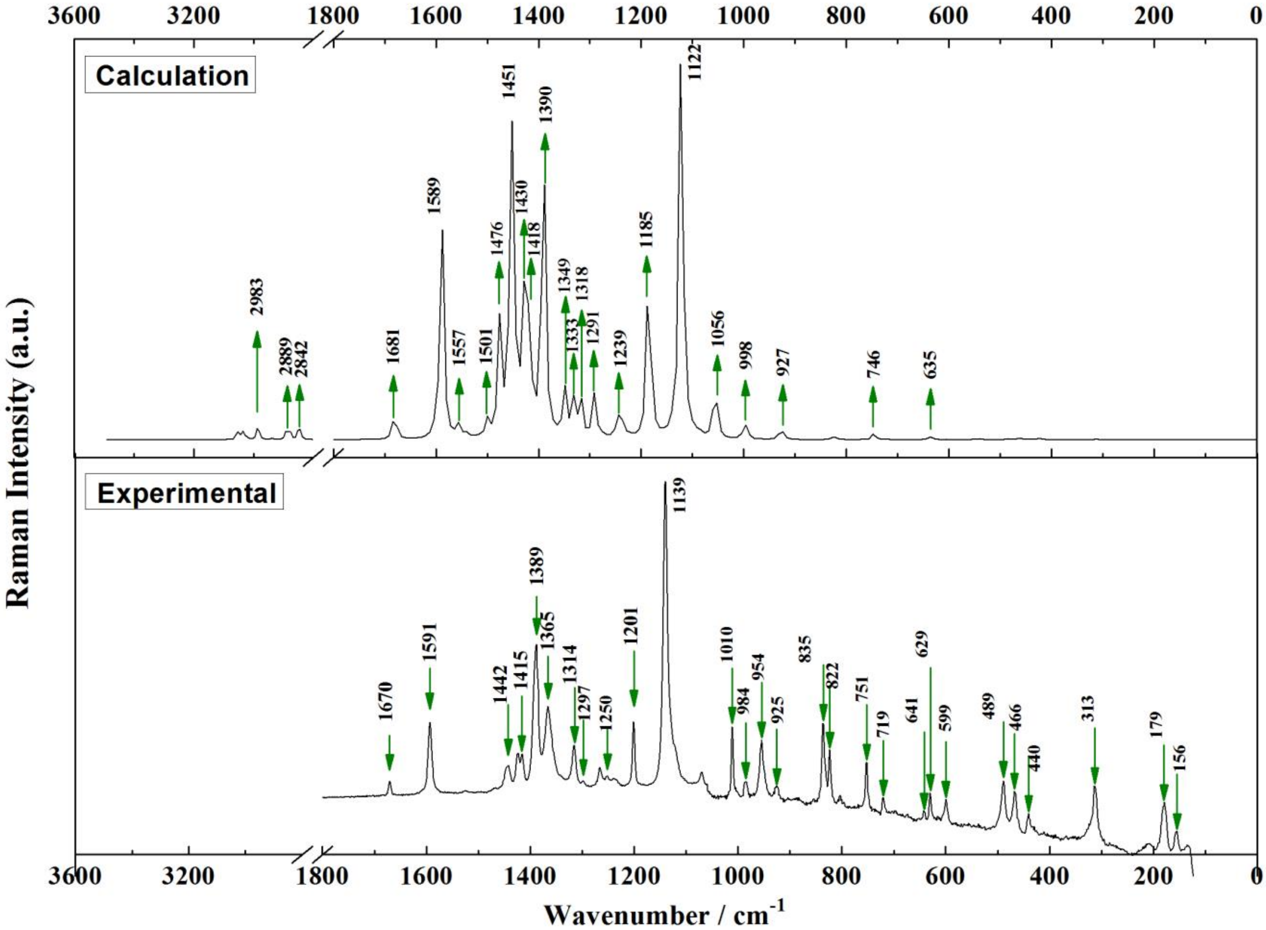

Figure 2. A comparison of the experimental (solid phase) Raman spectrum of DMA molecule with the calculated Raman spectrum obtained at the B3LYP/6-31+G(d,p) level of theory within the SQMFF methodology.

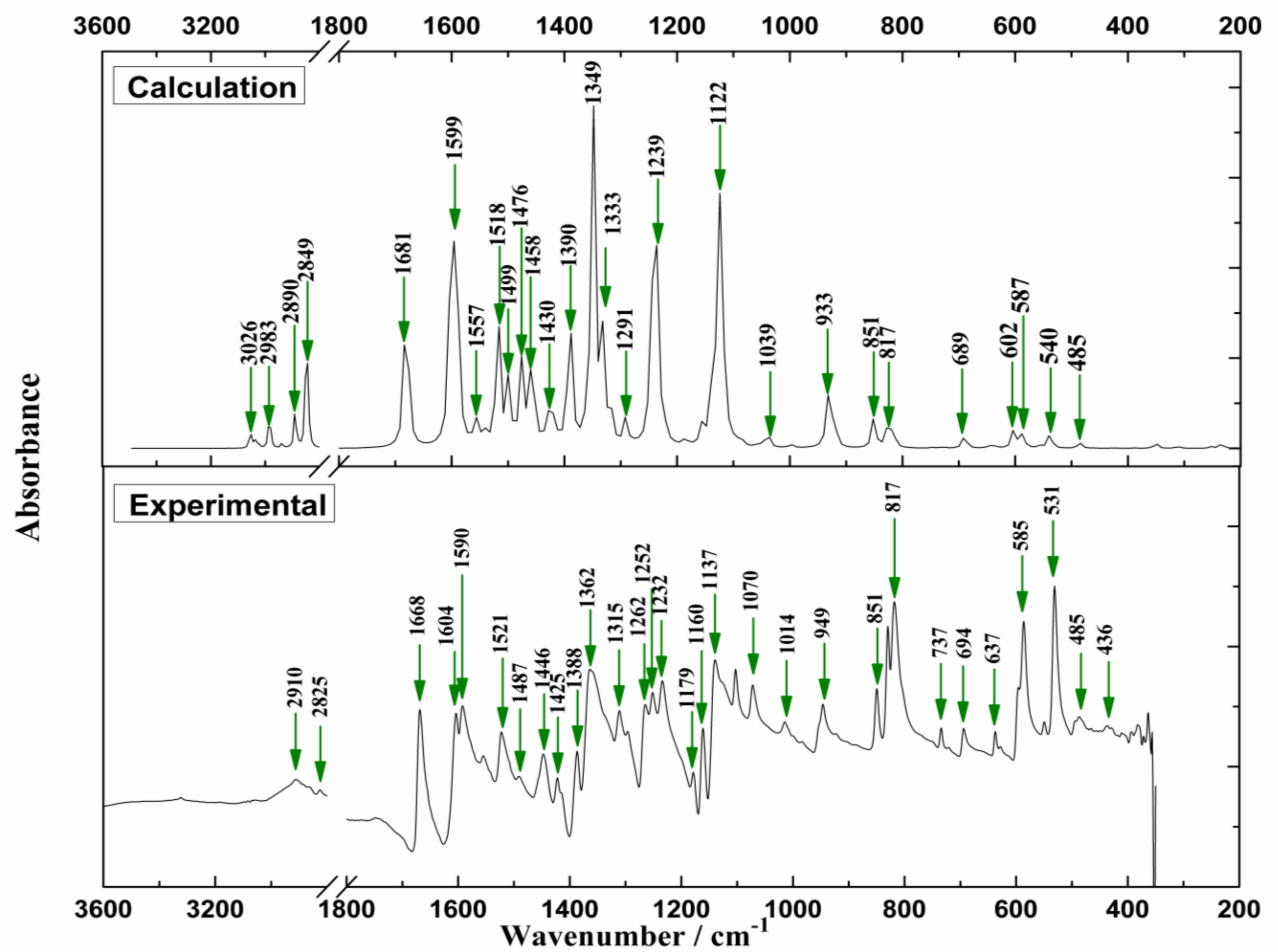

Figure 3. A comparison of the experimental (solid phase) IR spectrum of DMA molecule with the calculated IR spectrum obtained at the B3LYP/6-31+G(d,p) level of theory within the SQMFF methodology.

3.1.1. C-H vibrations

The aromatic C–H stretching vibrations are expected to appear wavenumber range 3100–3000 cm^{-1} [19]. Calculated SQM values of these bands at 3024 cm^{-1} to 3056 cm^{-1} are due to the C-H ring vibrations. C–H stretching vibrational modes in CH_3 groups are defined by the absorption bands in the 3000–2850 cm^{-1} range [19]. CH_3 symmetric stretching is assigned at 2910 cm^{-1}week band, while the calculated wavenumber is 2890 cm^{-1}.

3.1.2. N=N vibrations

Although azo compounds are no significant N=N stretching bands are expected in infrared spectroscopy, the N=N stretching band is generally strong intensity in Raman spectra [19]. Because of the azo compounds being non-polar in nature, the azo group is difficult to identify by infrared spectroscopy. In this study, N=N stretching vibrations are assigned 1368 cm^{-1} Raman and 1408 cm^{-1} and 1360 cm^{-1} IR [20]. The bands observed at 1488 cm^{-1} (IR), 1487 cm^{-1} (R), 1508 cm^{-1} (IR) and 1531 cm^{-1} (IR), 1532 cm^{-1} (R) in our before studies [21]. In this study, 1389 cm^{-1} strong Raman and 1425 cm^{-1} very weak IR band are observed, while the SQM 1418 cm^{-1}.

3.1.3. C-N vibrations

The characteristic functional of amine C-N range is expected 1240-1020 cm^{-1} [19]. The bands observed at very strong 1139 cm^{-1} and medium 1201 cm^{-1} Raman shift and also observed bands: 1179 cm^{-1}, 1160 cm^{-1}, 1137 cm^{-1} in the IR spectrum. The theoretically calculated CN vibrations (1122 cm^{-1}, IR and R, 1185 cm^{-1} medium IR and R) are in good agreement with the experimental bands.

Table 2. The assingments of the fundamental vibrations for the title molecule and comparison between the calculated DFT, SQM and observed experimental results

	B3LYP/ 6-31+G(d,p)			SQM			Observed[g]				
No	Freq[a]	I_{IR}[b]	I_{Raman}[c]	Freq[d]	I_{IR}[e]	I_{Raman}[f]	IR		Raman		TED(Total Energy Divibution)(>5%)[h]
105	3233	18.4	162.8	3056	18.3	162.3					CH sym v(95)
104	3230	12.3	52.2	3054	12.4	47.7					CH sym v(91)
103	3230	0.2	75.0	3053	0.1	79.9					CH sym v(95)
102	3216	3.2	54.6	3040	3.2	55.2					CH asym v(99)
101	3214	11.8	150.6	3039	11.8	150.2					CH sym v(98)
100	3211	1.2	75.5	3035	1.2	76.0					CH asym v(98)
99	3201	2.8	59.8	3026	2.8	59.7					CH asym v(99)
98	3199	6.1	57.6	3024	6.2	58.0					CH asym v(99)
97	3161	17.5	199.1	2988	17.4	199.2					CH3 asym v(100)
96	3156	43.5	270.2	2983	43.6	270.0					CH3 asym v(94)
95	3143	1.6	7.2	2971	1.6	7.3					CH3 asym v(93)
94	3108	8.4	51.0	2938	8.4	51.1					CH3 asym v(100)
93	3057	72.6	145.6	2890	72.7	145.7	2910	w			CH3 sym v(99)
92	3056	0.0	165.5	2889	0.0	165.0					CH3 asym v(100)
91	3045	3.5	252.3	2879	3.5	251.8					CH3 sym v(100)
90	3014	152.4	318.4	2849	151.3	319.1					CH3 sym v(94)
89	3007	91.7	192.8	2842	91.6	192.6	2825	vw			CH3 asym v(93)
88	1744	295.0	632.9	1681	286.1	617.4	1668	m	1670	w	CO v(83)
87	1658	518.5	316.9	1599	513.9	272.6	1604	m			CC v(55)
86	1647	138.5	4089.2	1589	162.7	4278.9	1590	m	1591	m	CC v(53) + NN v(5)
85	1610	24.9	106.7	1557	41.2	276.0					CC v(63)
84	1593	27.2	94.7	1543	26.5	107.0					CC v(60)
83	1559	354.4	73.4	1518	219.5	6.9	1521	m			CH3 b(50) + HCN b(17) + CN v(6)
82	1538	2.0	1271.2	1501	36.7	241.9					CH3 b(35)
81	1532	118.5	727.6	1499	72.4	92.3	1487	vw			HCH b(22)+NC v(9) +NN v(5)
80	1523	0.8	95.4	1478	14.8	36.0					HCH b(44)+HCNC t(21)
79	1501	185.9	1100.6	1476	119.1	2155.0					HCC b(18)+ NN v(15) + CC ring v(13)
78	1497	15.0	35.9	1469	0.0	7.2					CH3 b(58)
77	1493	18.8	215.5	1467	11.9	13.1					CH3 b(60)
76	1488	0.0	7.2	1458	134.1	1257.4					CH3 b(34)
75	1486	11.7	13.3	1456	13.9	75.2					CH3 b(63) + t(31)
74	1476	6.4	325.5	1451	14.4	6060.0	1446	vw	1442	w	NN v(15) + CC ring v(8)
73	1475	115.3	3765.5	1430	50.7	2769.4			1415	w	NN v(10) + CC ring v(7) + CH3 b(35)
72	1452	3.4	181.6	1418	46.7	2371.7	1425	vw	1389	s	NN v(8) + CC ring v(19) + t(35)
71	1440	171.8	4393.3	1390	239.6	6536.5	1388	vw			CC ring v(21) + HCC ip b(20) + NN v(16)
70	1396	503.6	828.6	1359	30.9	37.8	1362	m	1365	m	CH3 b(89)
69	1391	118.9	42.3	1349	549.6	907.7					CN v(37) + CC ring v(6)
68	1378	137.6	496.6	1333	169.7	673.8					CC ring v(62)
67	1365	36.8	725.8	1318	55.5	868.9	1315	w	1314	m	CC ring v(74)
66	1341	42.5	681.0	1291	42.9	882.9	1310	vw	1297	vw	HCC ring b(70)
65	1326	0.1	73.3	1274	2.2	60.6	1262	m			HCC ring b(73)
64	1293	10.9	204.6	1246	68.4	324.9	1252	m	1250	vw	CN v(24) + CC v(14)
63	1280	538.7	705.7	1239	517.7	423.4	1232	m	1240	vw	CN v(24) + CC v(26)
62	1274	77.4	159.0	1224	39.3	89.0					CN v(39) + CC v(22) + HCC(7) + HCN(5)
61	1229	1.8	2467.0	1185	11.7	3657.5	1179	w	1201	m	CN v(25) + CC v(14) + HCC ip b(6)
60	1198	46.3	14.8	1155	30.2	21.2	1160	w			HCN b(33) + CN v(8)
59	1185	133.6	73.3	1136	168.5	186.4	1137	m	1139	vs	CN v(8) + HCC ip b(34)
58	1165	510.4	25.9	1122	480.5	8284.2					CN v(17) + HCC ip b(27)
57	1148	15.7	311.8	1105	10.9	136.5					HCC ip b(58) + CC v(18)
56	1141	0.0	0.9	1096	0.0	1.0					HCN b(78)
55	1138	0.1	0.3	1092	0.2	0.5					HCN b(80)
54	1132	15.7	245.4	1088	12.4	100.2					CC ring v(22) + HCC ip b(58)
53	1089	3.1	608.9	1056	5.4	1099.5	1070	m			CC ring v(25) + CC v(10) + OCC b(7)+ CCC b(16)

Table 2. (Continued)

	B3LYP/ 6-31+G(d,p)			SQM			Observed[g]				
No	Freq[a]	I_{IR}[b]	I_{Raman}[c]	Freq[d]	I_{IR}[e]	I_{Raman}[f]	IR		Raman		TED(Total Energy Divibution)(>5%)[h]
52	1082	26.3	5.0	1039	26.2	5.1					HCN b(36) + CN v(29)
51	1044	0.6	0.4	1008	0.3	0.7	1014	vw	1010	m	HCC b(43) + t(37)
50	1022	2.7	251.5	998	5.1	297.7					HCC ring ip b(66) + CC(31)
49	1013	0.2	15.1	994	0.4	0.1					t(67) + HCC b(11)
48	1010	0.2	0.3	989	0.2	38.2			984	w	CCC ring op b(75) + CC ring v(21)
47	982	0.4	0.3	967	0.3	0.3					t(78)
46	977	0.2	0.8	962	0.1	0.7					t(81)
45	967	1.6	0.1	952	1.3	0.1			954	m	t(78)
44	964	38.0	7.6	933	69.2	27.0	949	m			CN v(32) + CNN b(14)
43	960	98.9	150.4	927	44.2	179.5			925	w	CC v(25) + HCC b(27)
42	937	0.5	20.2	919	24.1	19.5					CC v(28) + CNN b(24)
41	873	48.1	0.4	851	49.4	0.4	851	m			t ring op(76)
40	850	6.1	77.1	828	23.4	0.4			835	m	t ring breath(75)
39	849	20.5	0.4	824	6.5	66.7			822	m	CC v(36) + CN v(19) + CCC ring ip b(5)
38	837	37.8	0.0	817	33.6	0.0	817	vs			t ring op(62)
37	810	0.6	0.9	790	0.5	0.8					t ring op (93)
36	761	0.3	79.6	746	1.6	114.1			751		CN v(13) + CC v(11) + CCC ip ring(6)
35	745	2.0	0.5	728	2.1	0.3	737	w	719		t(6)
34	732	0.1	3.9	715	0.0	4.2					t(7)
33	707	23.6	1.8	689	22.9	1.2	694	w			CCC ring b ip(27) + CN b(27) + CC v(20)
32	653	4.1	2.5	646	4.4	2.7			641		CCC ring b ip(27)
31	642	2.3	43.2	635	2.8	48.4	637	w	629		CCC ring b ip (35)
30	608	36.1	2.3	602	34.5	3.1			599		CC v(18) + OCC b(33)
29	603	21.7	0.4	587	22.7	0.4	585	s			HCC b(13) + t(34)
28	559	4.2	1.8	557	3.7	3.3					NNC b(11) + CNC b(9) + NCC b(7) + OCC b(6)
27	548	13.5	1.9	540	12.1	14.4					NCC b(16) + CNC b(12) + NNC b(8) + OCC b(5)
26	541	12.3	14.8	537	12.7	1.8	531	s			t(37)
25	502	0.9	0.1	490	0.9	0.1			489		t inter ring(11)
24	488	9.4	15.1	485	7.9	12.9	485	w			CNC b(26) + CCC b(15) + OCC b(6) + NCC b(5)
23	466	0.5	36.3	462	0.4	35.0			466	w	CNC b(29) + NCC b(6) + NNC b(5) + OCC b(5)
22	446	0.0	0.3	435	0.0	0.3	436	vw	440	vw	tros(70)
21	426	0.9	23.8	424	0.9	30.0					CCC b(19) + CNC b(17) + OCC b(10) + NC v(6)
20	420	0.0	0.0	409	0.0	0.0					t(77)
19	396	0.5	0.7	387	0.5	0.7					t(43)
18	354	9.0	0.7	350	8.6	1.0					CC v(15) + CN v(6) + CCC b(12) + OCC b(11) + CNC b(8)
17	315	1.3	3.0	313	1.9	3.5			313	m	NCC b(43) + CNC b(20)
16	313	2.0	3.4	308	1.4	3.0					t(38)
15	257	2.5	0.3	251	2.5	0.4					CH3 t(60)
14	232	7.7	1.0	233	7.9	1.1					NCC b(28) + CCC b(26) + CNC b(19)
13	204	0.1	0.2	199	0.1	0.2					CH3 t(72)
12	188	6.1	1.4	186	6.5	1.9			179	w	CN v(14) + CNN b(6) + CCC b(26)
11	171	0.9	1.9	167	0.9	1.9					t(51)
10	162	0.1	0.2	157	0.1	0.2			156	vw	t(100)
9	147	0.8	1.7	147	0.6	2.0					NCC b(30) + NNC b(6) + CCC b(16)
8	143	0.5	0.9	140	0.5	0.8					t(45)
7	74	0.2	1.4	72	0.1	1.4					t(52)
6	69	1.4	0.3	68	1.6	0.3					t(40)
5	62	2.8	1.0	60	2.8	1.0					t(73)
4	48	0.5	0.9	49	0.5	0.9					CNN b(90)
3	41	0.8	1.9	40	0.8	1.9					t(63)
2	25	2.5	1.2	24	2.4	1.2					t(61)
1	18	0.1	0.3	18	0.1	0.3					t(80)

[a] Harmonic Vibrational Frequencies; [b] Infrared Intensities; [c] Raman Intensities;

[d]SQM Frequencies; [e]Infrared Intensities; [f]Raman Intensities; [g] vw, very weak; w, weak; m, medium; s,vong; vs, very vong

[h]The number after the modes are the % potential energy calculated using normal coordinate analysis; v, stretching; b, bending; t, torsion

3.2. Molecular electrostatic potential

The map of molecular electrostatic potential (MEP) surface visualizes the reactive sites of the DMA (in Fig. 4). The electrostatic potential increases red to blue potential region (red<orange<yellow<green<cyan<blue) positive and negative respectively. Map of electrostatic potential contour positive and negative potentials for the DMA compound are figured out in Fig. 5, at B3LYP/6-31+G(d,p) level.

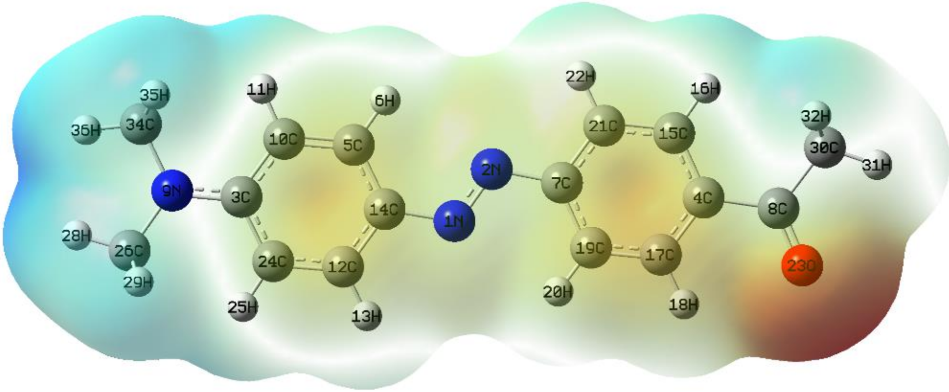

Figure 4. The 3D map of MEP surface of the DMA molecule.

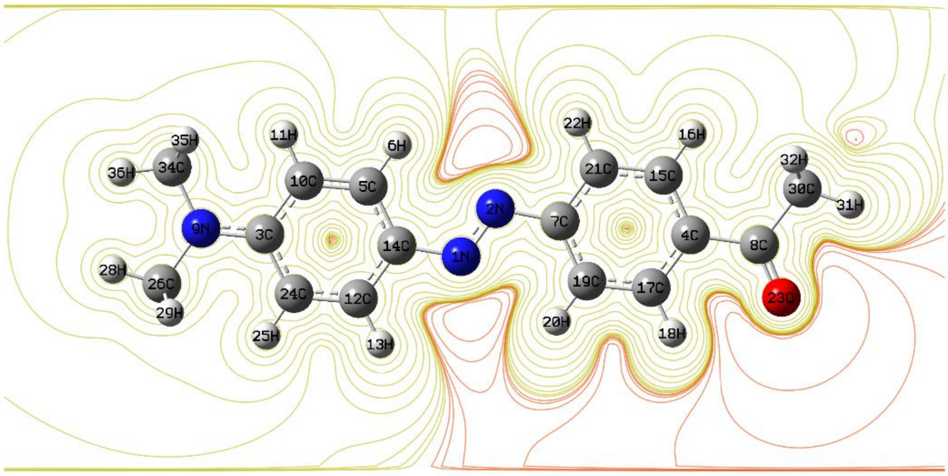

Figure 5. The 2D map of MEP contour of the DMA molecule.

4. Conclusions

The experimental and theoretical values of the vibrational frequencies of the studied molecule were compared. The RMS and mean average deviation of DMA fundamental vibrations were found as 7.46 and 3.78, respectively. This shows that the calcaulated frequencies are in good agreement with the experimental ones.

Acknowledgements

This study was supported by the Research Foundation of Mustafa Kemal University Project No: 15109. The author thanks to Zeynel Seferoğlu for his support giving permission to use the material, N,N-dimethylaniline. I would like to thank the Gazi University for providing Gaussian 09W Software. The numerical calculations reported in this paper were performed at TUBITAK ULAKBIM, High Performance and Grid Computing Center (TRUBA Resources).

References

[1] M. Neamtu, A. Yediler, I. Siminiceanu, M. Macoveanu, and A. Kettrup, “Decolorization of disperse red 354 azo dye in water by several oxidation processes - a comparative study,” *Dye. Pigment.*, vol. 60, no. 1, pp. 61–68, 2004.

[2] A. G. Tskhovrebov, L. C. E. Naested, E. Solari, R. Scopelliti, and K. Severin, “Synthesis of

azoimidazolium dyes with nitrous oxide," *Angew. Chemie - Int. Ed.*, vol. 54, no. 4, 2015.
[3] H. Valizadeh and A. Shomali, "A new nitrite ionic liquid (IL-ONO) as a nitrosonium source for the efficient diazotization of aniline derivatives and in-situ synthesis of azo dyes," *Dye. Pigment.*, vol. 92, no. 3, pp. 1138–1143, 2012.
[4] A. Matei, C. Constantinescu, B. Mitu, M. Filipescu, V. Ion, I. Ionita, S. Brajnicov, A. P. Alloncle, P. Delaporte, A. Emandi, and M. Dinescu, "Laser printing of azo-derivative thin films for non-linear optical applications," *Appl. Surf. Sci.*, vol. 336, pp. 200–205, 2015.
[5] S. Shahab, F. H. Hajikolaee, L. Filippovich, M. Darroudi, V. A. Loiko, R. Kumar, and M. Y. Borzehandani, "Molecular structure and UV–Vis spectral analysis of new synthesized azo dyes for application in polarizing films," *Dye. Pigment.*, vol. 129, pp. 9–17, 2016.
[6] Ö. Arslan, E. Yalçin, N. Seferoğlu, M. Yaman, and Z. Seferoğlu, "Molecular Structure Analysis and Spectroscopic Properties of Monoazo Disperse Dye From N , N -Dimethylaniline," vol. 30, no. 1, pp. 175–189, 2017.
[7] C. Y. Legault, "CYLview, 1.0b," *Univ. Sherbrooke*, p. http://www.cylview.org, 2009.
[8] M. Suhasini, E. Sailatha, S. Gunasekaran, and G. R. Ramkumaar, "Vibrational and electronic investigations, thermodynamic parameters, HOMO and LUMO analysis on Lornoxicam by density functional theory," *J. Mol. Struct.*, vol. 1100, pp. 116–128, Nov. 2015.
[9] M. J. et al Frisch, "Gaussian 09, Revision A.02," *Gaussian 09, Revision A.02*. 2009.
[10] G. Fogarasi, X. Zhou, P. W. Taylor, and P. Pulay, "The calculation of ab initio molecular geometries: efficient optimization by natural internal coordinates and empirical correction by offset forces," *J. Am. Chem. Soc.*, vol. 114, no. 21, pp. 8191–8201, 1992.
[11] P. Pulay, G. Fogarasi, G. Pongor, J. E. Boggs, and A. Vargha, "Combination of theoretical ab initio and experimental information to obtain reliable harmonic force constants. Scaled quantum mechanical (QM) force fields for glyoxal, acrolein, butadiene, formaldehyde, and ethylene," *J. Am. Chem. Soc.*, vol. 105, no. 24, pp. 7037–7047, 1983.
[12] P. Pulay, G. Fogarasi, F. Pang, and J. E. Boggs, "Systematic ab Initio Gradient Calculation of Molecular Geometries, Force Constants, and Dipole Moment Derivatives," *J. Am. Chem. Soc.*, vol. 101, no. 10, pp. 2550–2560, 1979.
[13] P. Pulay, G. Fogarasi, G. Pongor, J. E. Boggs, and A. Varghale, "Combination of Theoretical ab Initio and Experimental Information To Obtain Reliable Harmonic Force Constants . Scaled Quantum Mechanical (SQM) Force Fields for," *J. Am. Chem. Soc.*, vol. 105, no. Figure 3, pp. 7037–7047, 1983.
[14] J. Baker, A. A. Jarzecki, and P. Pulay, "Direct Scaling of Primitive Valence Force Constants: An Alternative Approach to Scaled Quantum Mechanical Force Fields," *J. Phys. Chem. A*, vol. 102, no. 8, pp. 1412–1424, 1998.
[15] "Parallel Quantum Solutions, SQM." Green Acres Road, Suite A, Fayetteville, AR 72703, 2013.
[16] P. Politzer, P. R. Laurence, and K. Jayasuriya, "Molecular electrostatic potentials: An effective tool for the elucidation of biochemical phenomena," *Environ. Health Perspect.*, vol. VOL. 61, no. 1, pp. 191–202, 1985.
[17] P. Politzer and J. S. Murray, "The fundamental nature and role of the electrostatic potential in atoms and molecules," *Theor. Chem. Acc.*, vol. 108, pp. 134–142, 2002.
[18] G. L. Hofacker, "Peter Politzer und Donald G. Truhlar: Chemical Applications of Atomic and Molecular Electrostatic Potentials, Plenum Press, New York und London 1981. 472 Seiten, Preis: $ 55.-," *Berichte der Bunsengesellschaft für Phys. Chemie*, vol. 86, no. 9, pp. 872–873, Sep. 1982.
[19] G. Socrates, *Infrared and Raman characteristic group frequencies*. 2004.
[20] B. Çatıkkaş, E. Aktan, and Z. Seferoğlu, "DFT, FT-Raman, FTIR, NMR, and UV-Vis studies of a hetarylazo indole dye," *Int. J. Quantum Chem.*, vol. 113, no. 5, pp. 683–689, Mar. 2013.
[21] E. Aktan, B. Babür, Z. Seferoğlu, T. Hökelek, and E. Şahin, "Synthesis and structure of a novel hetarylazoindole dye studied by X-ray diffraction, FT-IR, FT-Raman, UV–vis, NMR spectra and DFT calculations," *J. Mol. Struct.*, vol. 1002, no. 1–3, pp. 113–120, Sep. 2011.